International Journal of Solids and Structures 48 (2011) 2120–2130

Contents lists available at ScienceDirect

International Journal of Solids and Structures

journal homepage: www.elsevier.com/locate/ijsolstr

Magneto elastic stress subjected to uniform magnetic field over a thin infinite plate containing an elliptical hole with an edge crack

Norio Hasebe *

Department of Civil Engineering, Nagoya Institute of Technology, Gokiso-cho Showa-ku, Nagoya 466-8555, Japan
Nagoya Industrial Science Research Institute, Yotsuyadori 1-13, Chikusa-ku, Nagoya 464-0819, Japan

ARTICLE INFO

Article history:
Received 30 October 2010
Received in revised form 15 March 2011
Available online 23 March 2011

Keywords:
Magneto stress
Maxwell stress
Shear deflection
Magnetic field
Soft ferromagnetic material
Paramagnetic material
Elliptical hole
Edge crack
Stress intensity factor
Mapping function

ABSTRACT

Two dimensional solutions of the magnetic field and magneto elastic stress are presented for a magnetic material of a thin infinite plate containing an elliptical hole with an edge crack subjected to uniform magnetic field. Using a rational mapping function, each solution is obtained as a closed form. The linear constitutive equation is used for these analyses. According to the electro-magneto theory, only Maxwell stress is caused as a body force in a plate. In the present paper, it raises a plane stress state for a thin plate, the deformation of the plate thickness and the shear deflection. Therefore the magneto elastic stress is analyzed using Maxwell stress. No further assumption of the plane stress state that the plate is thin is made for the stress analysis, though Maxwell stress components are expressed by nonlinear terms. The rigorous boundary condition expressed by Maxwell stress components is completely satisfied without any linear assumptions on the boundary. First, magnetic field and stress analyses for soft ferromagnetic material are carried out and then those analyses for paramagnetic and diamagnetic materials are carried out. It is stated that those plane stress components are expressed by the same expressions for those materials and the difference is only the magnitude of the permeability, though the magnetic fields H_x, H_y are different each other in the plates. If the analysis of magnetic field of paramagnetic material is easier than that of soft ferromagnetic material, the stress analysis may be carried out using the magnetic field for paramagnetic material to analyze the stress field, and the results may be applied for a soft ferromagnetic material. It is stated that the stress state for the magnetic field H_x, H_y is the same as the pure shear stress state. Solutions of the magneto elastic stress are nonlinear for the direction of uniform magnetic field. Stresses in the direction of the plate thickness and shear deflection are caused and the solutions are also obtained. Figures of the magnetic field and stress distribution are shown. Stress intensity factors are also derived and investigated for the crack length.

1. Introduction

In the present paper, an infinite plate containing an elliptical hole with an edge crack exposed by magnetic field from out side of the plate are analyzed. In the previous paper (Hasebe, 2010a), the plate applied magnetic field induced by electric current was analyzed. Uniform magnetic field is one of the typical magnetic field as well as magnetic field caused by electric current. Main reviews have been stated in the previous paper; therefore the reviews are omitted for the limit pages.

Maxwell equations are essentially three dimensional ones for the magnetic field. Generally speaking, three dimensional boundary value problems are more difficult than those of two dimensional ones; therefore many problems have been modeled and analyzed as two dimensional problems. It seems not to be easy to make the two dimensional model of the magnetic field. However, when the plate is thin, the magnetic field in the plate with a hole can be obtained; therefore, the analysis is carried out for the thin plate, and also plane stress analysis can be applied.

According to the electro-magneto theory, only Maxwell stress components are caused as the body force in the magnetic material; therefore, Maxwell stress is considered for the stress analysis. No further assumptions for the magnetic stress analysis are made except the assumption of the plane stress state that the plate is thin, though Maxwell stress components and the boundary condition are expressed by the nonlinear terms of Maxwell stress components.

Intensities of the magnetic field component and stress intensity factors at the crack tip are obtained. The relationships among paramagnetic, diamagnetic and soft ferromagnetic materials are investigated for magneto elastic stress. Also the present problem causes shear deflection and the stress in the direction of the plate

* Address: Department of Civil Engineering, Nagoya Institute of Technology, Gokiso-cho Showa-ku, Nagoya 466-8555, Japan. Tel.: +81 52 876 5015.
E-mail address: hasebe@tea.ocn.ne.jp

0020-7683/$ - see front matter © 2011 Elsevier Ltd. All rights reserved.
doi:10.1016/j.ijsolstr.2011.03.017

thickness. In the previous paper, shear deflection does not arise. To the best of our knowledge, though the present problem is one of the fundamental problems, it seems not to have been solved analytically.

2. Preparation of problem and mapping function

The present study is shown in Fig. 1. The field of air surrounding the plate is called material 1, and the plate is called material 2, and the permeability is expressed by $\mu^{(1)}$ and $\mu^{(2)}$, respectively. The surfaces of the plate are named surfaces S_1, S_2 and S_3. The plate thickness is "h" which is assumed to be thin, and the elliptical hole has the semi-axes of "a" and "b", and the crack length is "c". The coordinates are denoted by x, y and z, respectively. The magnetic induction field of $\mathbf{B}_0$ Tesla applies to the entire plate from the outside of the plate, and the direction is γ radian from the x axis toward the counterclockwise direction, and the incident angle is α_1 radian from the vertical direction (see Fig. 3d). The magnetic induction field vector, $\mathbf{B}_0$, is expressed by the magnetic field intensity vector $\mathbf{H}_0$,

$$\mathbf{B}_0 = \mu^{(1)}\mathbf{H}_0 = \mu_0(1+\chi^{(1)})\mathbf{H}_0 \tag{1}$$

where μ_0: the magnetic permeability of free space (vacuum), $4\pi/10^7$ (NA^{-2}) and $\chi^{(1)}$: the magnetic susceptibility of material 1 (air).

To solve a problem shown in Fig. 1, the following rational mapping function is introduced:

$$w = \omega(\zeta) = F_0\zeta + \sum_{k=1}^{n=24}\frac{F_k}{\zeta_k-\zeta} + \frac{F_{25}}{\zeta} + F_c \tag{2}$$

where the complex variable "w" is defined as $w = x + iy$ to avoid confusion for "z" of the coordinates, and F_0, F_k ($k = 1,\ldots,25$) and F_c are constants, poles ζ_k ($k = 1,\ldots,24$) are located inside the unit circle, and $n = 24$ is used in this paper. This mapping function maps the exterior of the elliptical hole with an edge crack in the w-plane to the exterior of the unit circle in the ζ-plane shown in Fig. 2. The formulation is given in Hasebe and Horiuchi (1978), Hasebe and Inohara (1981) and Hasebe and Wang (2005).

When coefficients $F_k = 0$ ($k = 1,\ldots,24$) and $F_0 = (a+b)/2$ and $F_{25} = (a-b)/2$, the hole becomes an elliptical one where 'a' and 'b' are semi-axes of the elliptical hole. The magnitude of a radius, ρ, of curvature at the crack tip of (2) is $\rho/a = 10^{-9}$–10^{-11} which depends on the crack length and is very small. The radii of curvature at convex points K and H are also small, which is zero for an irrational mapping function.

One of the biggest merits using a rational mapping function is that stress functions achieved are exact ones for the geometrical shape represented by the rational function and a solution of a closed form can be obtained (Muskhelishvili, 1963). A rational mapping function of a sum of fraction expressions of (2) is also applied to any complicated configuration in principle (Hasebe and Horiuchi, 1978; Hasebe and Ueda, 1980; Hasebe et al., 1984). The technique can be also applied to a crack problem directly to calculate stress intensity factor.

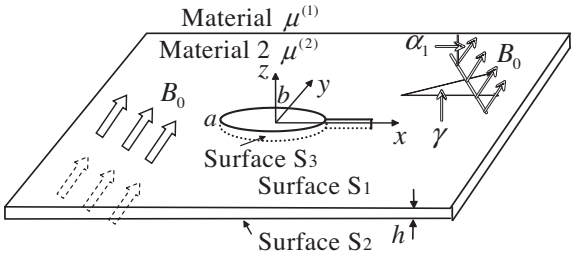

Fig. 1. Infinite thin plate containing an elliptical hole with an edge crack under uniform magnetic field with γ and α_1 directions.

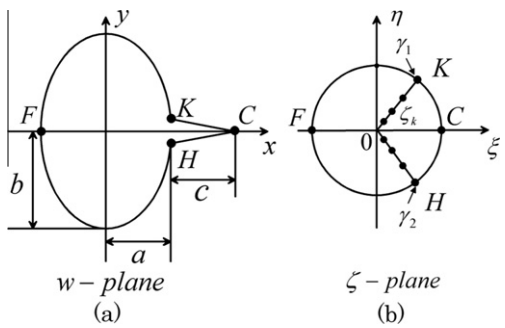

Fig. 2. Elliptical hole with an edge crack in an infinite plate and a unit circle.

3. Analysis of the magnetic field for a soft ferromagnetic material

The basic equations of the magnetic field in the thin plate ($|z| \leqslant h/2$) can be expressed by magnetic field intensity from Maxwell equations due to a linear constitutive equation as follows (Moon, 1984):

$$\begin{aligned}&\partial H_z/\partial y - \partial H_y/\partial z = 0, \quad \partial H_x/\partial z - \partial H_z/\partial x = 0,\\ &\partial H_y/\partial x - \partial H_x/\partial y = 0\end{aligned} \tag{3a, b, c}$$

$$\partial H_x/\partial x + \partial H_y/\partial y + \partial H_z/\partial z = 0 \tag{4}$$

In the previous paper (Hasebe, 2010a), the electric current terms exist on the right hand side of (3a, b) which is different from the present paper. In material 1, (3) and (4) must be also satisfied. These equations are solved under the following boundary conditions on the entire surfaces S_1, S_2 and S_3 between materials 1 and 2:

$$\begin{aligned}&(\mathbf{B}^{(2)} - \mathbf{B}^{(1)})\cdot\mathbf{n} = \left(\mu^{(2)}\mathbf{H}^{(2)} - \mu^{(1)}\mathbf{H}^{(1)}\right)\cdot\mathbf{n} = 0\\ &(\mathbf{H}^{(2)} - \mathbf{H}^{(1)})\times\mathbf{n} = 0\end{aligned} \tag{5a, b}$$

where $\mathbf{B}^{(2)}$, $\mathbf{H}^{(2)}$, $\mu^{(2)}$ and $\mathbf{B}^{(1)}$, $\mathbf{H}^{(1)}$, $\mu^{(1)}$ are the magnetic induction field, the magnetic field intensity and the magnetic permeability of materials 2 and 1, respectively; $\boldsymbol{n}$ is a unit normal vector at the interface. Eqs. (5a,b) denote the continuity of the magnetic induction field normal to and the magnetic field intensity tangential to the surface, respectively. The exact magnetic field problem is a three-dimensional one and is difficult to be solved exactly;

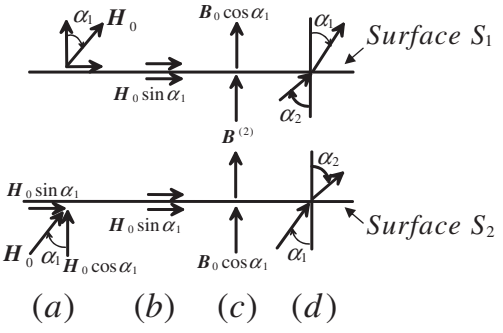

Fig. 3. Magnetic field on the surfaces; (a) magnetic field components on the surface; (b) horizontal magnetic field intensity; (c) vertical magnetic induction intensity; (d) incident and deflection angles.

therefore a few assumptions are made, appropriate for the kind of material. These assumptions are stated in Appendix A.

The magnetic field applied to the plate shown in Fig. 3a is decomposed in the magnetic field intensity parallel to the plate (Fig. 3b) and in the vertical magnetic induction field to the plate (Fig. 3c). The respective magnetic field is analyzed.

3.1. Analysis of magnetic field caused through surfaces S_1 and S_2

The magnetic field shown in Fig. 3b is analyzed. The magnetic field can be assumed $H_z(x,y,z) = 0(|z| \leqslant h/2)$ in the plate of a soft ferromagnetic material stated in Appendix A, and $H_x(x,y,z)$, $H_y(x,y,z)$ are uniform through the plate thickness, i.e., the components are not functions of variable z and are expressed by $H_x(x,y)$, $H_y(x,y)$. Therefore the basic equations from (3) and (4) are

$$\partial H_y/\partial x - \partial H_x/\partial y = 0, \quad \partial H_x/\partial x + \partial H_y/\partial y = 0 \tag{6a,b}$$

On surface S_3, the following boundary condition may be satisfied from (5a) under the condition $\mu^{(1)}/\mu^{(2)} \approx 0$ because $\mu^{(1)} \ll \mu^{(2)}$ for a soft ferromagnetic material:

$$\mathbf{H}^{(2)} \cdot \mathbf{n} \equiv H_r^{(2)} = 0 \tag{7}$$

Introducing the magnetic complex potential function $A(w) = A(\omega(\zeta)) \equiv A(\zeta)$ satisfying (6), the components of the magnetic field intensity are calculated from the following equation (Hasebe et al., 2007; Hasebe et al., 2008):

$$H_x(x,y) - iH_y(x,y) = -dA(w)/dw = -A'(\zeta)/\omega'(\zeta) \tag{8}$$

The boundary condition on surface S_3 is expressed as:

$$A(w) - \overline{A(w)} = A(\sigma) - \overline{A(\sigma)} = -2i \int \mathbf{H}^{(2)} \cdot \mathbf{n} ds + constant \tag{9}$$

where σ denotes ζ on the unit circle in the ζ plane and the bar above function denotes the conjugate function.

In the present problem, the magnetic field expressed by (A2) in Appendix A arises in the plate, and this magnetic field intensity has not satisfied the boundary condition (7). The magnetic complex potential function to be achieved is expressed as follows:

$$A(\zeta) = A_a(\zeta) + A_b(\zeta) \tag{10}$$

where the function, $A_a(\zeta)$, is given by (A2). Substituting the equation above into the boundary condition, (7) and (9), multiplying the resultant equation by $d\sigma/[2\pi i(\sigma - \zeta)]$, where ζ is a point outside of the unit circle, and applying the Cauchy integral on the unit circle in the clockwise direction, the function, $A_b(\zeta)$, is obtained as follows:

$$A_b(\zeta) = -H_0 \sin\alpha_1 \left[e^{-i\gamma} \left(\sum_{k=1}^{24} \frac{F_k}{\zeta_k - \zeta} + \frac{F_{25}}{\zeta} \right) - e^{i\gamma} \frac{F_0}{\zeta} \right] \tag{11}$$

where H_0 is the magnitude of the magnetic field intensity H_0. The constant term appearing in the equation above becomes zero because $A_b(\infty) = 0$ at the remote field. Therefore, (10) is expressed as

$$A(\zeta) = -H_0 F_0 \sin\alpha_1 \left(e^{-i\gamma}\zeta + e^{i\gamma}/\zeta \right) \tag{12}$$

where $F_0 = \overline{F}_0$.

Components of magnetic field intensity $H_r(\zeta)$ and $H_\theta(\zeta)$ normal and tangential to the curvilinear coordinates, respectively, expressed by the mapping function are calculated from the following equations:

$$H_r - iH_\theta = e^{i\beta}(H_x - iH_y), \quad e^{i\beta} = \zeta\omega'(\zeta)/|\zeta\omega'(\zeta)| \tag{13a,b}$$

3.2. Analysis of magnetic field caused through surface S_3

The boundary condition of (5b) on surface S_3 shown in Fig. 4 is given by

$$H_z^{(2)} = H_z^{(1)} = H_0 \cos\alpha_1 \tag{14}$$

From (5a) and $\mu^{(1)}/\mu^{(2)} \approx 0$, the components of the magnetic field intensity vertical to surface S_3 is zero on surface S_3 (see (7)), i.e.,

$$H_r^{(2)}(x,y) = 0 \tag{15}$$

In the equation above, the components on the surface S_3 may be uniform through the plate thickness, i.e. not functions of variable z. Because the boundary condition (14) of $H_z^{(2)}$ is uniform through the thickness of the plate and the plate thickness is thin, the component $H_z^{(2)}$ in the plate may be also assumed to be uniform through the plate thickness, i.e., not a function of the variable z, $\partial H_z/\partial z = 0$. From this condition and (4), the components $H_x^{(2)}$ and $H_y^{(2)}$ must satisfy (6) in the plate and the boundary condition (15). The solution is,

$$H_x^{(2)}(x,y) = H_y^{(2)}(x,y) = 0 \tag{16}$$

i.e., the components $H_x^{(2)}$ and $H_y^{(2)}$ do not arise through surface S_3.

Next the component $H_z^{(2)}$ caused through surface S_3 is determined from (3) and (4) and boundary condition (14). The following equations must be satisfied from (16), (3) and (4):

$$\partial H_z^{(2)}/\partial y = 0, \quad -\partial H_z^{(2)}/\partial x = 0, \quad \partial H_z^{(2)}/\partial z = 0 \tag{17a,b,c}$$

From (17) and (14), $H_z^{(2)}$ is obtained in the plate as follows:

$$H_z^{(2)} = H_0 \cos\alpha_1 \tag{18}$$

It is noticed that the magnetic field $H_z^{(2)}$ does not relate to the direction γ and is not caused in the plate for $\alpha_1 = \pi/2$. The equation $\mu^{(1)}H_z^{(1)} = \mu^{(2)}H_z^{(2)}$ holds on surfaces S_1 and S_2 (see (5a)); therefore

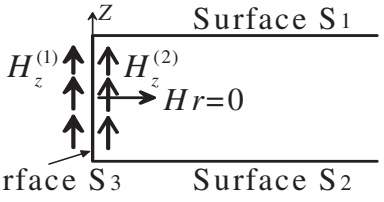

Fig. 4. Boundary condition of the magnetic field on surface S_3.

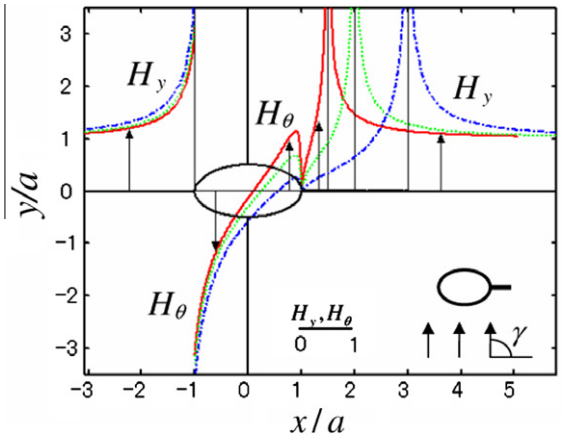

Fig. 5. Distributions of non-dimensional magnetic field H_y, $H_\theta/(H_0\sin\alpha_1)$ for $b/a = 0.5$: $c/a = 0.5$ (solid line), $c/a = 1$ (dotted line), $c/a = 2$ (dash-dotted line) and $\gamma = \pi/2$ along the x axis and the upper boundary surface.

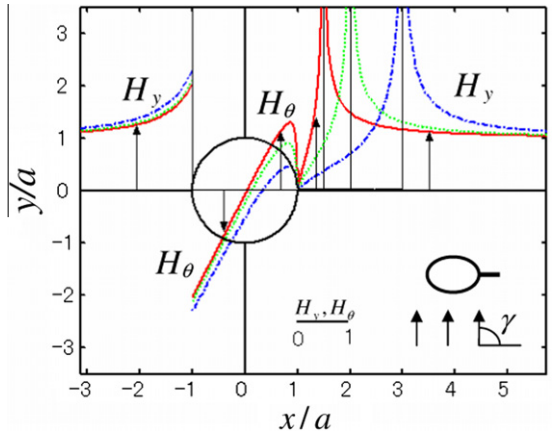

Fig. 6. Distributions of non-dimensional magnetic field H_y, $H_\theta/(H_0\sin\alpha_1)$ for $b/a = 1$: $c/a = 0.5$ (solid line), $c/a = 1$ (dotted line), $c/a = 2$ (dash-dotted line) and $\gamma = \pi/2$ along the x axis and the upper boundary surface.

$$H_z^{(1)} = \mu^{(2)} H_z^{(2)} / \mu^{(1)} \tag{19}$$

It is noticed that very large magnetic field intensity $H_z^{(1)}$ arises on the plate.

Figs. 5 and 6 show non-dimensional magnetic field for an elliptical hole with some crack lengths. The magnitude is shown by the distance from the axis. The magnetic field intensity, H_θ, along the elliptical hole is positive in the counterclockwise direction. The component H_θ is zero at the points $K(H)$ because of the convex corners. The concentration of H_y arises at the notch tip in Figs. 5 and 6 for $\gamma = \pi/2$. It is interesting that Fig. 5 in the present paper is the same form as that of the previous paper (electric current) (Hasebe, 2010a) except for the sign of H_x, H_y, H_θ because the direction of the magnetic field is different by 180° each other. The magnetic field $H_z^{(2)}$ is constant in the entire plate (see (18)) and is different from that of the electric current (Hasebe, 2010a).

4. Maxwell stress components and the discontinuous magnitude on the boundary surface

In the present paper, Maxwell stress for stress analysis is used for a soft ferromagnetic material (a linear magnetic material). The magnetic field influences the elastic body through the Lorentz body force in equilibrium equations (Paria, 1967; Moon, 1984).

$$\frac{\partial \sigma_{ik}}{\partial x_k} + ((\nabla \times \mathbf{H}) \times \mathbf{B})_i = 0$$
$$((\nabla \times \mathbf{H}) \times \mathbf{B})_i = ((\nabla \times \mathbf{H}) \times \mu \mathbf{H})_i \equiv \frac{\partial \bar{\tau}_{ik}}{\partial x_k} \quad (i,k = 1,2,3) \tag{20a, b}$$

where $\boldsymbol{B}$ is the magnetic induction field vector.

When the linear constitutive equation for the magnetic field is considered, Maxwell stress tensor, $\bar{\tau}_{ik}$, is expressed by the magnetic field intensity $\boldsymbol{H}$ as follows:

$$\bar{\tau}_{ik} = \mu \begin{vmatrix} 1/2(H_x^2 - H_y^2 - H_z^2) & H_x H_y & H_x H_z \\ H_y H_x & 1/2(H_y^2 - H_z^2 - H_x^2) & H_y H_z \\ H_z H_x & H_z H_y & 1/2(H_z^2 - H_x^2 - H_y^2) \end{vmatrix} \tag{21}$$

In the equation above, μ is the permeability of the magnetic material 2. In the following equations, the superscript (2) of μ for material 2 is omitted except for especial cases.

The components of magnetic field intensity H_x, H_y in the plate ($|z| \leqslant h/2$) are given by (12), (8) and $H_z(x,y)$ is given by (18). The discontinuous magnitude of Maxwell stress between materials 1 and 2 is expressed as follows (Hasebe, 2010a):

$$\begin{aligned} \mathbf{T}_{n1} - \mathbf{T}_{n2} &= (\mathbf{H}B_n)_1 - (\mathbf{H}B_n)_2 - \frac{1}{2}\{(\mathbf{H}\cdot\mathbf{B})_1 - (\mathbf{H}\cdot\mathbf{B})_2\}\mathbf{n} \\ &= \left\{\frac{B_n^2}{\mu^{(1)}}\mathbf{n} + \mathbf{H}_t B_n\right\}_1 - \left\{\frac{B_n^2}{\mu^{(2)}}\mathbf{n} + \mathbf{H}_t B_n\right\}_2 \\ &\quad - \frac{1}{2}\left\{\left(\frac{B_n^2}{\mu^{(1)}} + \mu^{(1)} H_t^2\right)_1 \mathbf{n} - \left(\frac{B_n^2}{\mu^{(2)}} + \mu^{(2)} H_t^2\right)_2 \mathbf{n}\right\} \\ &= \frac{1}{2}\left[\left(\frac{1}{\mu^{(1)}} - \frac{1}{\mu^{(2)}}\right) B_n^2 - (\mu^{(1)} - \mu^{(2)}) H_t^2\right]\mathbf{n} \equiv T_n \mathbf{n} \end{aligned} \tag{22}$$

where the direction of the positive normal vector $\mathbf{n}$ is one from materials 2 to 1 on the surface.

It is noticed that the direction of the discontinuous magnitude of Maxwell stress is normal to the surface. Each magnetic stress on surfaces S_3, S_1 and S_2 is presented as follows:

(a) Boundary surface S_3:
On surface S_3, the magnetic field intensities considering (7) are

$$B_n \equiv \mu^{(2)} H_r^{(2)} = 0, \quad H_t^2 = H_z^2 + H_\theta^2 \tag{23a, b}$$

where H_θ is the magnetic field intensity along the elliptical surface (see (13)), and $H_z (= H_z^{(2)})$ is the magnetic field intensity in the direction of the plate thickness on surface S_3 (see Fig. 4 and (14)). The discontinuous magnitude on surface S_3 is given from (22) and (23) by the following equation:

$$T_n = T_{n1} - T_{n2} = -\frac{1}{2}(\mu^{(1)} - \mu^{(2)})\left(H_t^2\right) \approx \frac{1}{2}\mu^{(2)}\left(H_z^2 + H_\theta^2\right) \tag{24}$$

where $\mu^{(1)} \ll \mu^{(2)}$ for a soft ferromagnetic materials. This magnetic stress component T_n exerts from materials 2 to 1 on surface S_3. Therefore the magnetic stress component applied to material 2 is $-T_n$.

(b) Boundary surfaces S_1 and S_2:
The magnetic field on surfaces S_1 and S_2 from (5), (8, 12) and (18) (see Figs. 3b and c) is

$$B_n = \mu^{(1)} H_z^{(1)} = \mu^{(2)} H_z^{(2)}, \quad H_t^2 = H_x^2 + H_y^2 \tag{25a, b}$$

These magnetic stress components contribute to the deformation of the plate thickness, because the magnitudes of (25) are the same values with the opposite direction on surfaces S_1 and S_2, respectively.

Figs. 7a and b show Maxwell stress components symmetric to and anti-symmetric to the $z = 0$ plane, respectively. All Maxwell stress components in the plate are not functions of variable z. The contribution of these Maxwell stresses to the deformation as the body force is investigated. The equilibrium Eq. (20) is divided to the following three equilibrium equations due to the contribution of Maxwell stress components to the deformation:

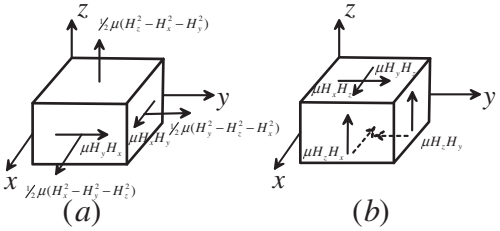

Fig. 7. Maxwell stress components.

State 1: The components $1/2\mu(H_x^2 - H_y^2 - H_z^2), 1/2\mu(H_y^2 - H_z^2 - H_x^2)$ and $\mu H_x H_y = \mu H_y H_x$ in Fig. 7a contribute to the plane elastic deformation (see (21)) and the magnetic stress on the boundary is given by (24). The shear stress components $\tau_{xz} = \tau_{yz} = 0$ symmetric to the $z = 0$ plane can be assumed, because the plate thickness is thin. Therefore the stress analysis is carried out as plane stress problem (generalized plane stress state) in the next section.

State 2: The component $1/2\mu(H_z^2 - H_x^2 - H_y^2)$ in Fig. 7a contributes to the deformation of the plate thickness. The boundary condition is given by (25) and the stress analysis is carried out in Section 6.

State 3: Maxwell stress components shown in Fig. 7b apply as the shear stress in the plate and cause the shear deflection of the thin plate. The stress analysis is carried out in section 7. This shear deflection does not arise in a plate under uniform electric current in the previous paper (Hasebe, 2010a).

It is necessary to state that the out of plate bending due to the bending moment is not caused by Maxwell stress shown in Fig. 7 and also the magnetic stress on the boundary (see (22)). Therefore the deflection of the plate in the present problem is caused only by the shear deflection mentioned in state 3.

5. Analysis of plane stress problem

For convenience, the plane stress problem is separated to two stress states and are analyzed for each problem, i.e., stress states (a) and (b) as follows (Hasebe, 2010a):

Stress state (a):

$$\begin{aligned}&\frac{\partial\sigma_x}{\partial x}+\frac{\partial\tau_{xy}}{\partial y}+\mu\left[\frac{1}{2}\frac{\partial}{\partial x}\left(H_x^2-H_y^2\right)+\frac{\partial}{\partial y}\left(H_xH_y\right)\right]=0\\&\frac{\partial\tau_{xy}}{\partial x}+\frac{\partial\sigma_y}{\partial y}+\mu\left[\frac{1}{2}\frac{\partial}{\partial y}\left(H_y^2-H_x^2\right)+\frac{\partial}{\partial x}\left(H_yH_x\right)\right]=0\end{aligned}\qquad(26a,b)$$

Stress state (b):

$$\begin{aligned}&\frac{\partial\sigma_x}{\partial x}+\frac{\partial\tau_{xy}}{\partial y}-\frac{1}{2}\mu\frac{\partial(H_z)^2}{\partial x}=0\\&\frac{\partial\tau_{xy}}{\partial x}+\frac{\partial\sigma_y}{\partial y}-\frac{1}{2}\mu\frac{\partial(H_z)^2}{\partial y}=0\end{aligned}\qquad(27a,b)$$

(a) Analysis of stress state (a)

When the following stress functions using the mapping function (2) are introduced,

$$\varphi_a(w)=\varphi_a[\omega(\zeta)]\equiv\Phi_a(\zeta),\quad \psi_a(w)=\psi_a[\omega(\zeta)]\equiv\Psi_a(\zeta)\qquad(28a,b)$$

the stress components are expressed as follows:

$$\begin{aligned}&\sigma_x+\sigma_y=4Re\left[\Phi_a'(\zeta)/\omega'(\zeta)\right]\\&\sigma_y-\sigma_x+2i\tau_{xy}=2\left[\overline{\omega(\zeta)}\left(\frac{\Phi_a'(\zeta)}{\omega'(\zeta)}\right)'\frac{1}{\omega'(\zeta)}+\frac{\Psi_a'(\zeta)}{\omega'(\zeta)}\right]+\mu(H_x-iH_y)^2\end{aligned}\qquad(29a,b)$$

The boundary equation is

$$\begin{aligned}\Phi_a(\sigma)+\omega(\sigma)\overline{\frac{\Phi_a'(\sigma)}{\omega'(\bar\sigma)}}+\overline{\Psi_a(\sigma)}&=\frac{1}{2}\left(\mu^{(1)}-\mu^{(2)}\right)\int H_\theta^2\omega'(\sigma)d\sigma\\&=\frac{1}{2}\left(\mu^{(1)}-\mu^{(2)}\right)\int\overline{(H_x-iH_y)^2\omega'(\sigma)d\sigma}\\&=\frac{1}{2}\left(\mu^{(1)}-\mu^{(2)}\right)\int\overline{\left[-\frac{A'(\sigma)}{\omega'(\sigma)}\right]^2\omega'(\sigma)d\sigma}\end{aligned}\qquad(30)$$

where σ denotes a coordinate on the unit circle in the ζ-plane. The function $A(\zeta)$ is expressed by (12).

Multiplying $d\sigma/[2\pi i(\sigma-\zeta)]$ to (30), and carrying out Cauchy integration on the unit circle, the following equation is obtained:

$$\begin{aligned}\Phi_a(\zeta)&=-\sum_{k=1}^{24}\frac{F_k}{\zeta_k-\zeta}\overline{\frac{\Phi_a'(\zeta_k')}{\omega'(\zeta_k')}}+1/2\left(\mu^{(1)}-\mu^{(2)}\right)H_0^2F_0\sin^2\alpha_1e^{2i\gamma}/\zeta\\&\approx-\sum_{k=1}^{24}\frac{F_k}{\zeta_k-\zeta}\overline{\frac{\Phi_a'(\zeta_k')}{\omega'(\zeta_k')}}-1/2\mu^{(2)}H_0^2F_0\sin^2\alpha_1e^{2i\gamma}/\zeta\end{aligned}\qquad(31)$$

where $\left(\mu^{(1)}-\mu^{(2)}\right)\approx-\mu^{(2)}$, and $\mu^{(1)}\ll\mu^{(2)}$ was used. This Cauchy integration of the right hand side of (30) and unknowns $\overline{\Phi_a'(\zeta_k')}$are decided solving $2n = 48$ simultaneous equation (Hasebe, 2010a; Hasebe et al., 2007).

Another stress function is obtained from analytic continuation of (30) as

$$\begin{aligned}\Psi_a(\zeta)=&-\overline{\Phi_a}\left(\frac{1}{\zeta}\right)-\bar\omega(1/\zeta)\frac{\Phi_a'(\zeta)}{\omega'(\zeta)}\\&+\frac{1}{2}\left(\mu^{(1)}-\mu^{(2)}\right)\int(H_x-iH_y)^2\omega'(\sigma)d\sigma\end{aligned}\qquad(32)$$

As mentioned in Appendix B, it is interesting to notice that the stress states of (29), (31) and (32) are the same as the pure shear stress state (Hasebe and Ueda, 1980).

Stress components for an arbitrary direction γ of the magnetic field can not be obtained by the composition of the individual stress components of, for example, $\gamma = 0$ and $\pi/2$ because the direction of magnetic field is expressed by$e^{2i\gamma}$.

The stress components σ_θ, σ_r, $\tau_{r\theta}$ tangential and normal to the curvilinear coordinates expressed by the mapping function (2) are calculated from

$$\begin{aligned}&\sigma_\theta+\sigma_r=\sigma_x+\sigma_y\\&\sigma_\theta-\sigma_r+2i\tau_{r\theta}=e^{2i\beta}(\sigma_y-\sigma_x+2i\tau_{xy})\end{aligned}\qquad(33a,b)$$

where $e^{2i\beta}$ is the square of (13b).

(b) Analysis of stress state (b)

The stress analysis of stress state (b) is carried out by a similar way to stress state (a). Introducing the mapping function (2) and stress functions $\Phi_b(\zeta)$ and $\Psi_b(\zeta)$, stress components are expressed as follows:

$$\begin{aligned}&\sigma_x+\sigma_y=4Re\left[\Phi_b'(\zeta)/\omega'(\zeta)\right]+\mu(H_z)^2\\&\sigma_y-\sigma_x+2i\tau_{xy}=2\left[\overline{\omega(\zeta)}\left(\frac{\Phi_b'(\zeta)}{\omega'(\zeta)}\right)'\frac{1}{\omega'(\zeta)}+\frac{\Psi_b'(\zeta)}{\omega'(\zeta)}\right]\end{aligned}\qquad(34a,b)$$

and the stress boundary condition is expressed by

$$\begin{aligned}\Phi_b(\sigma)+\omega(\sigma)\overline{\frac{\Phi_b'(\sigma)}{\omega'(\sigma)}}+\overline{\Psi_b(\sigma)}&=\frac{1}{2}\left(\mu^{(1)}-\mu^{(2)}\right)\int[H_z]^2\omega'(\sigma)d\sigma\\&=1/2\left(\mu^{(1)}-\mu^{(2)}\right)H_0^2\cos^2\alpha_1\omega(\sigma)\end{aligned}\qquad(35)$$

Multiplying $d\sigma/[2\pi i(\sigma-\zeta)]$ to (35), and carrying out Cauchy integration on the unit circle, the following equation is obtained:

$$\begin{aligned}\Phi_b(\zeta)=&-\sum_{k=1}^{24}\frac{F_k}{\zeta_k-\zeta}\overline{\frac{\Phi_b'(\zeta_k')}{\omega'(\zeta_k')}}+1/2\left(\mu^{(1)}-\mu^{(2)}\right)H_0^2\\&\times\cos^2\alpha_1\left(\sum_{k=1}^{24}\frac{F_k}{\zeta_k-\zeta}+\frac{F_{25}}{\zeta}\right)\\\approx&-\sum_{k=1}^{24}\frac{F_k}{\zeta_k-\zeta}\overline{\frac{\Phi_b'(\zeta_k')}{\omega'(\zeta_k')}}-1/2\mu^{(2)}H_0^2\cos^2\alpha_1(\omega(\zeta)-F_0\zeta)\end{aligned}\qquad(36)$$

where $(\mu^{(1)} - \mu^{(2)}) \approx -\mu^{(2)}$. The unknown constant $\overline{\Phi_b'(\zeta_k')}$ is determined by similar way to the stress state (a) (Hasebe, 2010a; Hasebe et al., 2007).

Another stress function is obtained from analytic continuation of (35) as

$$\Psi_b(\zeta) = -\bar{\Phi}_b(1/\zeta) - \bar{\omega}(1/\zeta)\frac{\Phi_b'(\zeta)}{\omega'(\zeta)} - \frac{1}{2}\mu^{(2)}H_0^2\cos^2\alpha_1\bar{\omega}(1/\zeta) \tag{37}$$

Or multiplying $d\sigma/[2\pi i(\sigma-\zeta)]$ to the conjugate equation of (35), and carrying out Cauchy integration on the unit circle, the following equation is obtained:

$$\Psi_b(\zeta) = -\frac{\bar{\omega}(1/\zeta)}{\omega'(\zeta)}\Phi_b'(\zeta) + \sum_{k=1}^{24}\frac{\overline{F}_k\zeta_k'^2}{\zeta-\zeta_k'}\frac{\Phi'(\zeta_k')}{\omega'(\zeta_k')} - \frac{1}{2}\mu^{(2)}H_0^2\cos^2\alpha_1\frac{F_0}{\zeta} \tag{38}$$

Eqs. (37) and (38) are the same equations, and do not include the direction γ. The stress components are calculated from (34), and those of the curvilinear coordinates expressed by the mapping function are calculated by (33).

The final plane stress state is obtained by the superposition of stress states (a) and (b). When the incident angle,$\alpha_1 = 0$, $H_x = H_y = 0$ from (8) and (12). Therefore stress state (a) does not arise in the plate. When the incident angle, $\alpha_1 = \pi/2$, $H_z = 0$ from (18). Therefore stress state (b) does not arise in the plate.

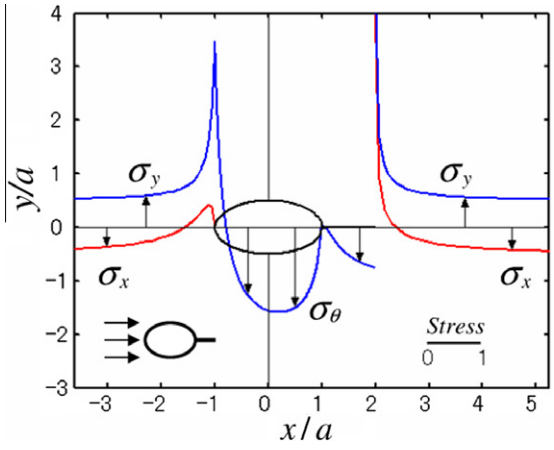

Fig. 8. Nondimensional stress distributions $\sigma_\theta, \sigma_x, \sigma_y/\left\{\mu H_0^2\sin^2\alpha_1\right\}$ of stress state (a) for $\gamma = 0$ and $b/a = 0.5$ the upper surface of the elliptical hole with crack length $c/a = 1$ and along the x axis.

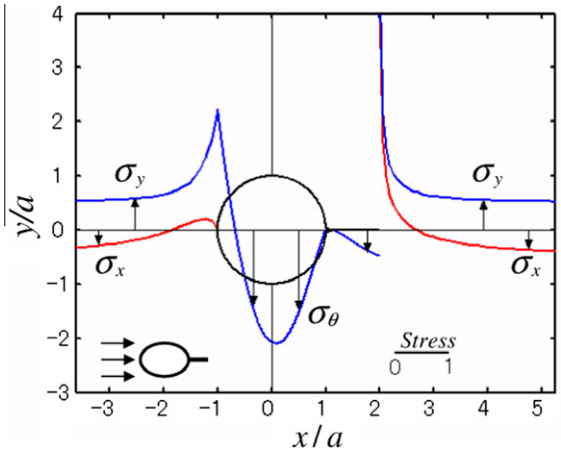

Fig. 9. Nondimensional stress distributions $\sigma_\theta, \sigma_x, \sigma_y/\left\{\mu H_0^2\sin^2\alpha_1\right\}$ of stress state (a) for $\gamma = 0$ and $b/a = 1$ along the upper surface of the circular hole with crack length $c/a = 1.0$ and along the x axis.

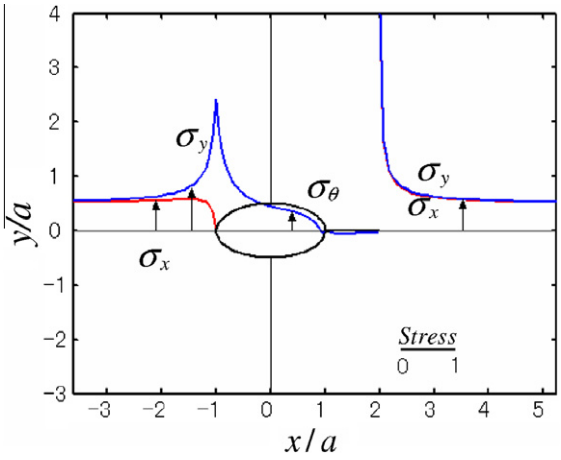

Fig. 10. Nondimensional stress distributions $\sigma_\theta, \sigma_x, \sigma_y/\left(\mu H_0^2\cos^2\alpha_1\right)$ of stress state (b) for $b/a = 0.5$ along the upper surface of the elliptical hole with crack length $c/a = 1.0$ and along the x axis.

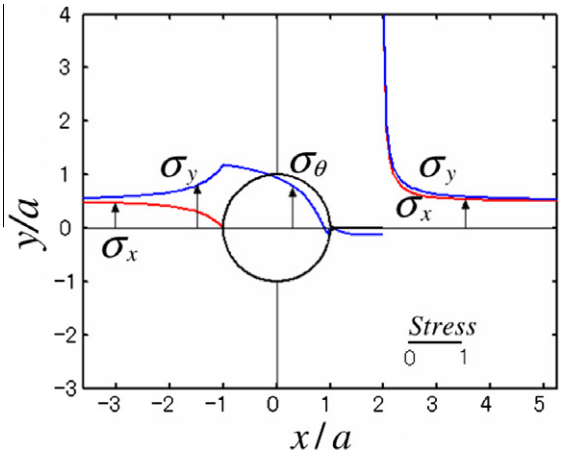

Fig. 11. Nondimensional stress distributions $\sigma_\theta, \sigma_x, \sigma_y/\left(\mu H_0^2\cos^2\alpha_1\right)$ of stress state (b) for $b/a = 1.0$ along the upper surface of the circular hole with crack length $c/a = 1.0$ and along the x axis.

Figs. 8 and 9 show the non-dimensional stress distribution for $\gamma = 0$ along the x axis and the upper surface of the elliptical hole with a crack for stress state (a). The stress distributions at the remote area are tensile and compressive stresses $\sigma_x, \sigma_y/\mu H_0^2\sin^2\alpha_1 = \pm 0.5$ in the direction of the x axis, respectively. It coincides with Faraday Law of the electric power line. This stress state presents the pure shear stress state (see Appendix B). Therefore the non-dimensional stress distribution under the magnetic field caused by uniform electric current and uniform magnetic field in the present case takes same form because the same magnetic fields arise (Hasebe, 2010a). Figs. 10 and 11 show the stress distribution of stress state (b) due to the magnetic field $H_z(x,y)$. There are stress concentrations at the crack tip. The stress distributions at the remote area are tensile stresses $\sigma_x, \sigma_y/\mu H_0^2\cos^2\alpha_1 = +0.5$ in the direction of the x axis.

6. Stress in the direction of the plate thickness

Because $\tau_{zx} = \tau_{zy} = 0$ is assumed when the plate thickness is thin, the equation contributing to the deformation of the plate thickness is expressed by (see Fig. 7a) (Hasebe, 2010a),

$$\frac{\partial \sigma_z}{\partial z}+\frac{\partial \bar{\tau}_{zz}}{\partial z}=\frac{\partial \sigma_z}{\partial z}+\frac{1}{2}\mu^{(2)}\frac{\partial (H_z^2-H_x^2-H_y^2)}{\partial z}=0 \tag{39}$$

The variation of the magnetic momentum on the boundary surfaces S_1 and $S_2(|z| = \pm h/2)$ is

$$\sigma_z+\mu^{(2)}\left(H_z^2-H_x^2-H_y^2\right)/2+T_n=p_z(=0)$$
$$T_n=T_{n1}-T_{n2}=\left(1/\mu^{(1)}-1/\mu^{(2)}\right)\left(\mu^{(2)}H_z^{(2)}\right)^2/2 \tag{40a, b}$$
$$-\left(\mu^{(1)}-\mu^{(2)}\right)\left(H_x^2+H_y^2\right)/2$$

where external force $p_z = 0$ in the present problem and the magnetic stress, T_n, is given by (22). From (39) and (40), the stress component σ_z in the plate is expressed by

$$\sigma_z=-(\mu^{(2)})^2H_z^2/(2\mu^{(1)})+\mu^{(1)}\left(H_x^2+H_y^2\right)/2$$
$$\approx -(\mu^{(2)})^2H_0^2\cos^2\alpha_1/(2\mu^{(1)}) \tag{41}$$

where $\mu^{(1)} \ll \mu^{(2)}$ is used.Stress σ_z is very strong compressive stress in the plate, because the permeability of air $\mu^{(1)}$ is very small (see (1)). When the incident angle $\alpha_1 = \pi/2$, the magnetic field intensity in the plate is $H_z = 0$, and σ_z is almost zero because $\mu^{(1)}$ is very small (see the second term of the second equation of (41)).

7. Analysis of the shear deflection

In the previous paper of the electric current, the shear deflection does not arise. In the present paper, the shear deflection arises, and the derivation is carried out. The equilibrium equations due to Maxwell shear stress components anti-symmetric to the z plane (see Fig. 7b) can be written from (20) and (21) as follows:

$$\frac{\partial}{\partial z}(\tau_{xz}+\mu H_xH_z)=0,\quad \frac{\partial}{\partial z}(\tau_{yz}+\mu H_yH_z)=0$$
$$\frac{\partial}{\partial x}(\tau_{zx}+\mu H_zH_x)+\frac{\partial}{\partial y}(\tau_{zy}+\mu H_zH_y)=0 \tag{42a, b, c}$$

Because Maxwell shear stress μH_zH_x and μH_zH_y are not functions of variable z, components τ_{zx}, τ_{zy} are not functions of variable z from (42a, b), i.e., uniform through the plate thickness. The problem of (42) is an anti-plane shear stress problem (longitudinal shear stress problem) (Hasebe et al., 1986a). When the magnetic shear stress terms are expressed by

$$\tau_{zxs}\equiv\tau_{zx}+\mu H_zH_x,\quad \tau_{zys}\equiv\tau_{zy}+\mu H_zH_y \tag{43a, b}$$

the variation of the magnetic momentum on the boundary (stress boundary condition) is

$$\tau_{zxs}dy+\tau_{zys}(-dx)=\tau_{zr}ds(=0) \tag{44}$$

where τ_{zr} is the external shear stress on the boundary, and $\tau_{zr} = 0$ in the present case. The magnetic shear force does not apply on the boundary surface S_3 (see (23)); therefore the solution is $\tau_{zxs} = \tau_{zys} = 0$, that is,

$$\tau_{zx}=-\mu H_zH_x,\quad \tau_{zy}=-\mu H_zH_y \tag{45a, b}$$

The shear stress τ_{zx}, τ_{zy} of (45) satisfies the boundary condition ($\tau_{zr} = 0$) on surface S_3 because $H_r^{(2)}=0$ is satisfied (see (7)). When the shear deflection is expressed by $w_s(x,y)$, the shear stress components are expressed by

$$\tau_{zx}=G\partial w_s/\partial x,\quad \tau_{zy}=G\partial w_s/\partial y \tag{46a, b}$$

where G is the shear modulus. The shear deflection $w_s(x,y)$ is confirmed to be a harmonic function from (42c) and (46), because (6b) and (17) holds. Therefore introducing a complex potential function $S(w) = S(\omega(\zeta)) \equiv S(\zeta)$, the shear stress components and the shear deflection are expressed using (45), (46a,b) and (8) as follows:

$$\tau_{zx}-i\tau_{zy}=GdS(w)/dw=GS'(\zeta)/\omega'(\zeta)=\mu H_z^{(2)}A'(\zeta)/\omega'(\zeta)$$
$$w_s=\left[S(\zeta)+\overline{S(\zeta)}\right]/2 \tag{47a, b}$$

The function,$S(\zeta)$, is derived by the integral of (47a):

$$S(\zeta)=\mu^{(2)}H_z^{(2)}A(\zeta)/G$$
$$=-\mu^{(2)}H_0^2\sin\alpha_1\cos\alpha_1F_0(e^{-i\gamma}\zeta+e^{i\gamma}/\zeta)/G \tag{48}$$

The defection angle at infinity becomes constant value, but the shear deflection becomes infinite, because the plate is infinite, and the deflection is anti-symmetric to, for example, the y axis for$\gamma = 0$. It is noticed from (47b), (48), (14) and (12) that when the incident angle $\alpha_1 = \pi/4$, the shear deflection and shear stresses are maximum.

The shear stress components $\tau_{z\theta}$, τ_{zr} tangential and normal to the curvilinear coordinates, respectively, expressed by the mapping function (2) are calculated from

$$\tau_{zr}-i\tau_{z\theta}=e^{i\beta}(\tau_{zx}-i\tau_{zy}) \tag{49}$$

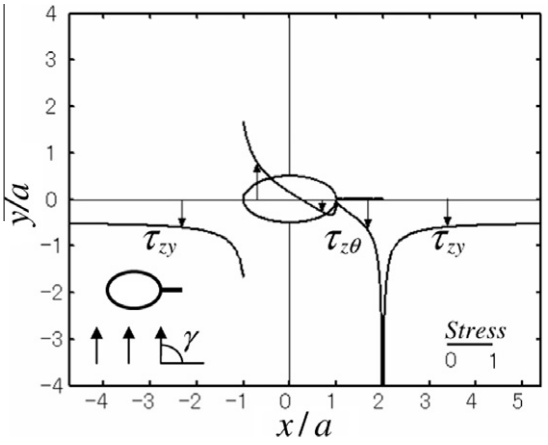

Fig. 12. Non-dimensional shear stress distributions $\tau_{z\theta}, \tau_{zy}/\left(\mu H_0^2\sin 2\alpha_1\right)$ of shear deflection for $\gamma = \pi/2$ and $b/a = 0.5$ along the upper surface of the elliptical hole with crack length $c/a = 1.0$ and along the x axis.

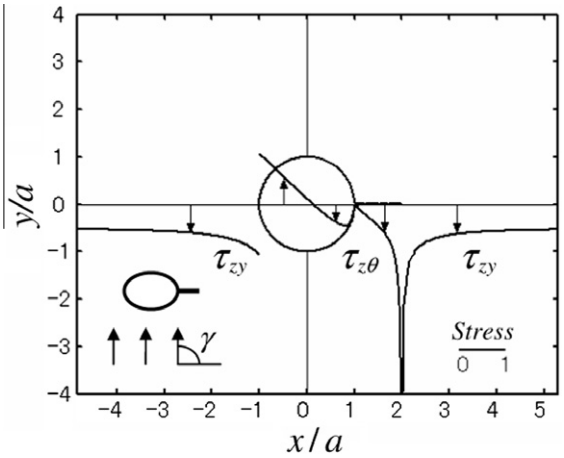

Fig. 13. Non-dimensional shear stress distribution $\tau_{z\theta}, \tau_{zy}/\left(\mu H_0^2\sin 2\alpha_1\right)$ of shear deflection for $\gamma = \pi/2$ and $b/a = 1.0$ along the upper surface of the circular hole with crack length $c/a = 1.0$ and along the x axis.

where $e^{i\beta}$ is given by (13b). The positive direction of $\tau_{z\theta}$ is the counterclockwise direction. Figs. 12 and 13 show distributions of non-dimensional shear stress component. There is a stress concentration of τ_{zy} at the elliptical tip. The stress component is zero at points K (H), because these points are convex corners.

8. Intensity factor at the crack tip and the magnitude of stress

It is noticed from (8) that the magnetic field intensities $H_x(x,y)$, $H_y(x,y)$ have the singularity and is the same as that of the electric current at the crack tip (Hasebe, 2010a). The components near the crack tip for a ferromagnetic material are given by the following equations:

$$H_x(x,y)=\frac{H_f}{\sqrt{2\pi r}}\sin\frac{\theta}{2},\quad H_y(x,y)=-\frac{H_f}{\sqrt{2\pi r}}\cos\frac{\theta}{2} \tag{50a, b}$$

where r is the distance from the crack tip and θ is the angle measured in the counterclockwise direction. The intensity H_f is obtained using the magnetic complex potential function $A(\zeta)$, (8), as follows:

$$H_f=i\sqrt{\pi}A'(\zeta_0)/\sqrt{e^{i\lambda_1}\omega''(\zeta_0)}=-2\sqrt{\pi}F_0H_0\sin\alpha_1\sin\gamma\sqrt{2\pi a}/\sqrt{2\omega''(\zeta_0)}$$
$$H_f=\tilde{H}_fH_0\sin\alpha_1\sin\gamma\sqrt{2\pi a} \tag{51a, b}$$

where λ_1 is the angle between the x axis and crack direction, and ζ_0 is the coordinate at the crack tip, and $\lambda_1=0$, and $\zeta_0=1$ in the present case. The coefficient $\tilde{H}_f$ is the non-dimensional intensity. It is noticed that the intensity H_f is maximum for $\gamma=\pi/2$, i.e., the magnetic field is vertical to the crack direction.

Fig. 14 shows the non-dimensional intensity $\tilde{H}_f$ versus the crack length,c/a, for some elliptical holes. Though the value of H_f is minus, the value of $H_y(x,y)$ is plus at the crack tip (see (50b) and Fig. 5). The line of $\tilde{H}_{feq}$is the intensity for the equivalent crack length $2a_{cr}=(2a+c)$, and is defined as follows:

$$H_{feq}=-\tilde{H}_{feq}H_0\sin\alpha_1\sin\gamma\sqrt{2\pi a}$$
$$\tilde{H}_{feq}=\sqrt{1+c/(2a)}/\sqrt{2} \tag{52a, b}$$

The difference among values $\tilde{H}_f$ and $\tilde{H}_{feq}$ shows the effect of the hole.

The magnetic field intensity $H_z(x,y)$ does not take any singularity at the crack tip (see (18)).

Stress components have a stress singularity at the crack tip. The stress intensity factors (SIF), K_{Ia}, K_{IIa} for stress state (a) are calculated by the following equations using (31):

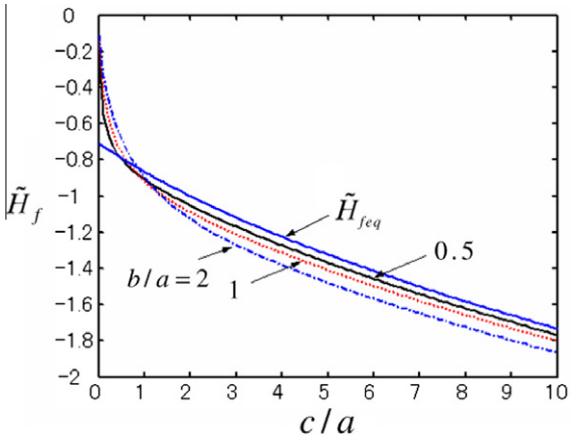

Fig. 14. Non-dimensional magnetic field intensity versus crack length c/a for $b/a=0.5$ (solid line), $b/a=1$ (dotted line), $b/a=2$ (dash-dotted line) and equivalent intensity $\tilde{H}_{feq}$ for crack length $2a_{cr}=(2a+c)$.

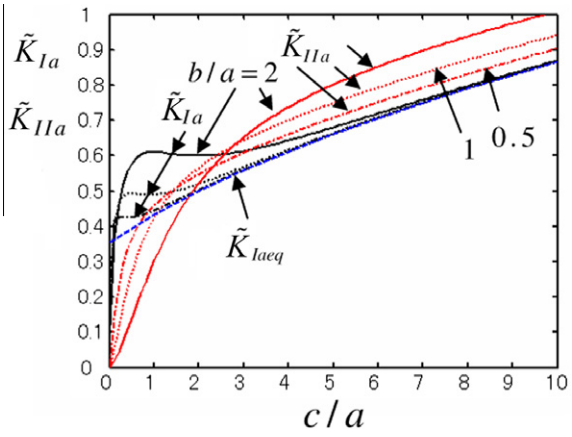

Fig. 15. Non-dimensional stress intensity factor Modes I and II versus crack length c/a for stress state (a): $b/a=0.5$ (dash-dotted lines), $b/a=1$ (dotted lines), $b/a=2$ (solid lines) and equivalent stress intensity factor $\tilde{K}_{Iaeq}$ for crack length $2a_{cr}=(2a+c)$.

$$K_{Ia}-iK_{IIa}=2\sqrt{\pi}\Phi_a'(\zeta_0)/\sqrt{e^{i\lambda_1}\omega''(\zeta_0)}$$
$$\tilde{K}_{Ia}=K_{Ia}/\left[\mu^{(2)}H_0^2\sin^2\alpha_1\cos2\gamma\sqrt{2\pi a}\right] \tag{53a, b, c}$$
$$\tilde{K}_{IIa}=-K_{IIa}/\left[\mu^{(2)}H_0^2\sin^2\alpha_1\sin2\gamma\sqrt{2\pi a}\right]$$

where $\tilde{K}_{Ia}$, $\tilde{K}_{IIa}$ are the non-dimensional stress intensity factors and $\mu^{(1)}/\mu^{(2)}\approx0$ was used.

Fig. 15 shows non-dimensional SIF for stress state (a) and the line of $\tilde{K}_{Iaeq}$ is that for the equivalent crack length $2a_{cr}=(2a+c)$. The equivalent SIF is defined (Hasebe, 2010b) as follows:

$$K_{Iaeq}=\tilde{K}_{Iaeq}\mu^{(2)}H_0^2\sin^2\alpha_1\cos2\gamma\sqrt{2\pi a}$$
$$K_{IIaeq}=-\tilde{K}_{IIaeq}\mu^{(2)}H_0^2\sin^2\alpha_1\sin2\gamma\sqrt{2\pi a} \tag{54a, b, c, d}$$
$$\tilde{K}_{Iaeq}=\sqrt{1+c/(2a)}/2\sqrt{2}$$
$$\tilde{K}_{IIaeq}=\sqrt{1+c/(2a)}/2\sqrt{2}$$

The SIF increases with the crack length; therefore, once a crack starts to propagate, it does not stop. Modes I and II SIF change with $\cos2\gamma$ and $\sin2\gamma$ for the magnetic field direction, respectively. When the direction of the uniform magnetic field is $\gamma=0$ and $\gamma=\pi/4$, the K_{Ia} and K_{IIa} take the maximum value, respectively. The difference between SIF and $\tilde{K}_{Iaeq}$ shows the effect of the elliptical hole. These SIF are the same as those of SIF of the uniform electric current (Hasebe, 2010a).

The SIF for stress state (b) can be obtained using the stress function $\Phi_b(\zeta)$ in (53a), and are given by

$$K_{Ib}=\tilde{K}_{Ib}\mu H_0^2\cos^2\alpha_1\sqrt{2\pi a},\quad K_{IIb}=0 \tag{55a, b}$$

The equivalent SIF K_{Ibeq} is defined for the equivalent crack length $2a_{cr}=(2a+c)$ as follows:

$$K_{Ibeq}=\tilde{K}_{Ibeq}\mu H_0^2\cos^2\alpha_1\sqrt{2\pi a},$$
$$\tilde{K}_{Ibeq}=\sqrt{1+c/(2a)}/2\sqrt{2} \tag{56a, b}$$

Fig. 16 shows non-dimensional SIF for stress state (b) and the line $\tilde{K}_{Ibeq}$. Values K_{Ib} are always positive for any incident angle α_1 except $\alpha_1=\pi/2$, and does not relate to the direction γ. Values K_{IIb} are always zero.

The total stress intensity factors K_I and K_{II} are given by the superposition of stress states (a) and (b). The SIF of stress states (a) and (b) have the same order in magnitude (see Figs. 15 and 16). When $\gamma=0$, the $K_I=K_{Ia}+K_{Ib}$ value takes maximum value. The K_{II} value is maximum when angle $\gamma=\pi/4$ and $\alpha_1=\pi/2$.

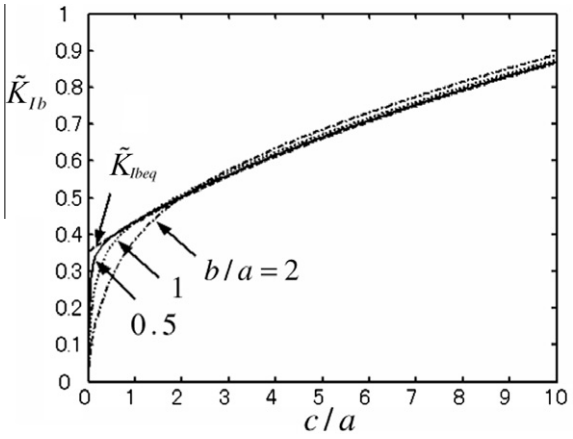

Fig. 16. Non-dimensional Mode I stress intensity factors for stress state (b) versus crack length c/a for $b/a = 0.5$ (solid line), $b/a = 1$ (dotted line), $b/a = 2$ (dash dotted line) and equivalent stress intensity factor $\tilde{K}_{Ibeq}$ for crack length $2\ a_{cr} = (2a + c)$.

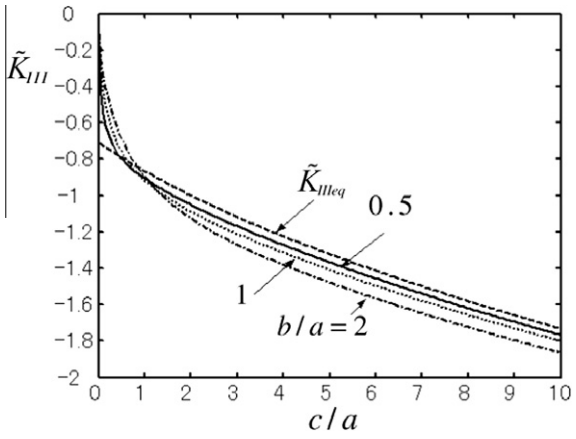

Fig. 17. Non-dimensional Mode III stress intensity factors versus crack length c/a for $b/a = 0.5$ (solid line), $b/a = 1$ (dotted lines), $b/a = 2$ (dash dotted lines) and equivalent stress intensity factor $\tilde{K}_{IIIeq}$ for crack length $2a_{cr} = (2a + c)$.

In the present problem, the shear stress components cause Mode III SIF which is (Hasebe et al., 1986a)

$$K_{III} = i\sqrt{\pi}GS'(\zeta_0)/\sqrt{\omega''(\zeta_0)} = \tilde{K}_{III}\mu H_0^2 \sin\ 2\alpha_1 \sin\gamma\sqrt{2\pi a} \tag{57}$$

When $\alpha_1 = 0,\ \pi/2$, the K_{III} does not arise. Also when $\gamma = 0$, the K_{III} does not arise due to the symmetry to the x axis. When $\alpha_1 = \pi/4$ and $\gamma = \pi/2$, it takes the maximum value. Fig. 17 shows the non-dimensional SIF of Mode III. It is interesting that this figure is the same as Fig. 14 because $A(\zeta)$ is the same.

It is important to investigate the magnitude of stress in the plate exposed by the given uniform magnetic field. At the remote field of the plate of stress state (a), the stress component is given by $\sigma_y = \mu^{(2)}H_0^2/2 = \mu_0(1+\chi^{(2)})(B_0/\mu_0)^2/2 \approx \chi^{(2)}B_0^2/(2\mu_0)$ using (1) for $\gamma = 0$ and $\alpha_1 = \pi/2$ (see Figs. 8, 9 and (B3)). For example, when steel of susceptibility $\chi^{(2)} = 10^3$ and 10^4, and $B_0 = 1$ Tesla (the saturation is around 2 Tesla) are considered, $\sigma_y \approx 0.4 \times 10^3$ and 4×10^3 MPa, respectively, and this value is comparable magnitude in engineering, because the Yield stress of steel is around $1.4 - 2.0 \times 10^3$ MPa. Similar investigation can be carried out for stress state (b).

Maxwell stress components have a singularity of order $1/r$ at the crack tip as noticed from (50) and (21). However as stated in Appendix B, stress components in stress state (a) do not positively include Maxwell stress components, and thus the singularity of order $1/r$ does not appear at the crack tip. For stress state (b), Maxwell stress component $H_z^2(x,y)$ does not include any singularity.

9. Stress for paramagnetic, diamagnetic and soft ferromagnetic materials

In the previous paper of uniform electric current, the relationships among paramagnetic, diamagnetic and soft ferromagnetic materials were investigated. Therefore it is also interesting and important to investigate the relationship of magneto elastic stress under uniform magnetic field among paramagnetic, diamagnetic, and ferromagnetic materials. First, the magnetic field in the plate of the paramagnetic, diamagnetic materials is investigated. The permeability $\mu^{(2)}$ of the paramagnetic and diamagnetic material is almost the same as that of material 1 (air), i.e., $\mu^{(2)} \approx \mu^{(1)}$. Therefore the magnetic field in paramagnetic and diamagnetic materials is the same as that of the magnetic field of material 1 (air) due to the boundary condition (5). The magnetic fields in the plate are given by (see (A2) and Fig. 3)

$$H_x^{(2)} = H_0 \sin\alpha_1 \cos\gamma, \quad H_y^{(2)} = H_0 \sin\alpha_1 \sin\gamma$$
$$H_z^{(2)} = H_0 \cos\alpha_1 \tag{58a, b, c}$$

The magnetic fields H_x, H_y are different from, but H_z are the same as those of a soft ferromagnetic material, respectively (see (8, 12) and (18)).

The boundary condition of stress state (a) for paramagnetic and diamagnetic materials is the same equation as (30) (see (B1)):

$$\Phi_a(\sigma) + \omega(\sigma)\frac{\overline{\Phi_a'(\sigma)}}{\omega'(\sigma)} + \overline{\Psi_a(\sigma)} = \frac{1}{2}(\mu^{(1)} - \mu^{(2)})\int \overline{(H_x - iH_y)^2\omega'(\sigma)d\sigma} \tag{59}$$

The stress functions are obtained from this boundary using (58) as follows:

$$\Phi_a(\zeta) = -\sum_{k=1}^{24}\frac{F_k}{\zeta_k - \zeta}\frac{\overline{\Phi_a'(\zeta_k')}}{\overline{\omega'(\zeta_k)}} + 1/2(\mu^{(1)} - \mu^{(2)})H_0^2 \sin^2\alpha_1 F_0 e^{2i\gamma}/\zeta$$

$$\begin{aligned}\Psi_a(\zeta) &= -\overline{\Phi_a}\left(\frac{1}{\zeta}\right) - \frac{\bar{\omega}(1/\zeta)}{\omega'(\zeta)}\Phi_a'(\zeta) \\ &\quad + \frac{1}{2}(\mu^{(1)} - \mu^{(2)})\int (H_x - iH_y)^2\omega\prime(\sigma)d\sigma \\ &= -\overline{\Phi_a}\left(\frac{1}{\zeta}\right) - \frac{\bar{\omega}(1/\zeta)}{\omega'(\zeta)}\Phi_a'(\zeta) \\ &\quad + \frac{1}{2}(\mu^{(1)} - \mu^{(2)})H_0^2 \sin^2\alpha_1 e^{-2i\gamma}\omega(\zeta)\end{aligned} \tag{60a, b}$$

(60a) is the same form as (31). Because stress components are expressed by (B3) in Appendix B, the expressions for stress component for paramagnetic, diamagnetic and soft ferromagnetic material are the same ones except that the magnitude of the permeability $\mu^{(2)}$ is only different. This fact was already stated in Hasebe et al. (2007); Hasebe (2010a).

The boundary condition of stress state (b) for paramagnetic and diamagnetic materials is also given by (35). Therefore the stress functions are the same as those of soft ferromagnetic material. Naturally because the magnetic field (18) and the boundary condition are the same ones for paramagnetic, diamagnetic and soft ferromagnetic materials, the same magnetic stresses can be obtained. The only difference is the magnitude of permeability of the materials among these materials. Therefore from the discussion above the distinction among paramagnetic, diamagnetic and soft ferromagnetic materials is unnecessary for the analyses of the plane stress state, though the magnetic fields H_x, H_y are different for each material. This fact comes from that the constitutive equation of the

magnetic material is a linear one. If to obtain the magnetic and stress fields of a paramagnetic material is easier than that of a soft ferromagnetic material, the analyses may be carried out using the magnetic field of a paramagnetic material and then the results can be applied to a soft ferromagnetic material.

Analysis of shear deflection for paramagnetic and diamagnetic materials can be carried out by the same way as section 7 and the same form solution can be obtained for stress components. However the magnetic fields H_x, H_y are different from those of a soft ferromagnetic material.

The stress component σ_z is derived by the same way as that in section 6. It is

$$\sigma_z = -(\mu^{(2)})^2 H_z^2/(2\mu^{(1)}) + \mu^{(1)}\left(H_x^2 + H_y^2\right)/2 \approx -\mu^{(1)}\left[H_z^2 - H_x^2 - H_y^2\right]/2 \tag{61}$$

The first equality is the same form as that of (54). However the function of the magnetic field H_x, H_y is different from that of soft ferromagnetic material. Therefore the distributions are different for the respective materials. However in case of a soft ferromagnetic material, the second term can be neglected. The magnitude of σ_z for paramagnetic and diamagnetic materials is extremely small and can be neglected in engineering side.

10. Conclusions

Using a rational mapping function, the analyses of the magneto elastic field and the magnetic stress were carried out. The closed form solutions were obtained for each problem. If $F_k = 0$ ($k = 1,2,\ldots,n$ (=;24)) are taken in these solutions, the solutions for an elliptical hole can be obtained. When the semi-axes$a = 0$, $b \neq 0$, and the crack length $c \neq 0$, solutions of a T shaped crack can be obtained for each problem. If the coefficients of the mapping function (2) are changed, other geometric shapes can be analyzed, for examples, a square hole with a crack (Hasebe and Ueda, 1980), and a kinked crack (Hasebe and Inohara, 1981; Hasebe et al., 1986b). The radius of curvature at the crack tip is very small; therefore the stress intensity factor can be calculated directly from the stress function. This is one of the merits of a rational mapping function of the present paper.

The magneto elastic stress analysis using Maxwell stress is straightforward and acceptable, because according to the electromagneto theory, only Maxwell stresses are caused as the body force in the magnetic material. Except for the approximation of the plane stress state in which the plate is thin, no further assumptions for the stress analysis are made, though Maxwell stresses and the boundary condition are expressed by nonlinear terms due to Maxwell stress components. The boundary condition expressed by Maxwell stress is the precise boundary condition which is completely satisfied without any linear assumptions on the boundary.

Maxwell stress components in the present problem cause the shear deflection as well as the plane stress state and the stress component σ_z. From the stress analysis which was carried out for soft ferromagnetic, paramagnetic and diamagnetic materials, as the result, the expressions of stress for those materials for plane stress state are the same ones, though the respective magnetic fields, H_x, H_y, are different. This mechanical truth comes from a linear magnetic material. If to obtain the magnetic field of a paramagnetic material is easier than that of a soft ferromagnetic material, the stress analysis may be carried out using the paramagnetic field of the paramagnetic material, and then the solution can be applied to a soft ferromagnetic material.

The stress of σ_z are different for respective materials, but is strong compressive stress in the plate for a soft ferromagnetic material. The magnetic field intensity $H_z^{(1)}(x,y)$ is very large in the plate (see (19)).

The magnetic fields in the plate consist of those through surfaces S_1 and S_2 and through surface S_3. The magnetic field is essentially three dimensional one; therefore, the precise two-dimensional magnetic field in the plate is necessary to analyze the two-dimensional magneto elastic problem.

Stress state (a) caused by the magnetic field H_x, H_y is the same as that of uniform shear stress state. Therefore, the stress functions of stress state (a) for a thin plate with a hole of an arbitrary shape under uniform magnetic field are given by the stress functions with uniform shear stress $-\mu H_0^2(\sin\alpha_1)^2/2 \equiv \tau_0$ at the remote field. Stress components for an infinite plate with an arbitrary shaped hole can be obtained from Hasebe et al. (2001, 2007) or for example, (Hasebe and Ueda, 1980) for pure shear stress analysis. Or superposition of stress states subject to compression in the direction of magnetic field and tension in the perpendicular to the magnetic field at the remote field. This fact coincides with Faraday's law of electric power line.

The SIF for stress state (a) are given by (53), and take maximum values when the incident angle$\alpha_1 = \pi/2$. When angle$\gamma = 0$, K_{Ia} also takes a maximum value. Stress components and SIF for an arbitrary direction of the magnetic field cannot be obtained by the composition of the individual direction, for example, $\gamma = 0$ and $\pi/2$.

Stress state (b) is caused by the $H_z(x,y)$ magnetic field. The stress order of Stress states (a) and (b) is the same one in the magnitude, and the magnetic stress was investigated for steel as an example, and the comparable stress is caused in magnitude in engineering.

The shear deflection is caused for any incident angle (oblique magnetic field to the plate) except $\alpha_1 = 0$ and $\pi/2$, and the analysis is carried out as an anti-plane shear problem. The shear stress deflection takes the maximum value for$\alpha_1 = \pi/4$, and produces Mode III SIF which takes maximum value at the angle $\alpha_1 = \pi/4$. An out of a thin plate bending deflection due to the bending moment does not arise under uniform magnetic field.

Magnetic fields H_x, H_y have a singularity of order $1/\sqrt{r}$ at the crack tip, but magnetic field $H_z(x,y)$ does not have a singularity at the crack tip and takes a finite value. The singularity of order $1/r$ does not appear in the stress components, though Maxwell stress components H_x^2, H_y^2 have a singularity of order $1/r$, because Maxwell stress terms do not appear in the stress components.

The saturation of the magnetic field has not been considered due to the assumption of the linear constitutive equation. The range of the application of the linear magnetic stress analysis depends on the magnetic materials. The linear magneto elastic stress analysis can be seen as an analogue to the elastic analysis for the real elastic–plastic materials.

Appendix A. Magnetic field in the plate caused through surfaces S_1 and S_2 at the remote field

The derivation is written in Hasebe et al. (2008) and Hasebe (2010a), therefore; the only results are shown as follows.

At the remote field of the plate, the following magnetic fields arise in the plate from the boundary condition of surfaces S_1 and S_2 (see Fig. 3)

$$H_{xa}(x,y) = H_0 \sin\alpha_1 \cos\gamma, \quad H_{ya}(x,y) = H_0 \sin\alpha_1 \sin\gamma \tag{A1a, b}$$

where the subscript, "a", is used to avoid confusion. The components of (A1) are expressed by the function, $A_a(\zeta)$, defined by (8) as follows:

$$H_{xa}(x,y,z) - iH_{ya}(x,y,z) = H_0 \sin\alpha_1(\cos\gamma - i\sin\gamma) = -A_a'(\zeta)/\omega'(\zeta)$$
$$A_a(\zeta) = -H_0 \sin\alpha_1 e^{-i\gamma}\omega(\zeta) \tag{A2a, b}$$

Appendix B. Stress of stress state (a)

The first term in the right hand side of (30) is written as follows:

$$
\begin{aligned}
-\frac{1}{2}\mu\int H_\theta^2 dw &= \frac{1}{2}\mu\int e^{-2i\beta}(H_x+iH_y)^2 dw \\
&= \frac{1}{2}\mu\int \frac{\bar\sigma\overline{\omega'(\sigma)}}{\sigma\omega'(\sigma)}(H_x+iH_y)^2\omega'(\sigma)d\sigma \\
&= -\frac{1}{2}\mu\int \overline{\omega'(\sigma)}(H_x+iH_y)^2\left(-\frac{1}{\sigma^2}\right)d\sigma \\
&= -\frac{1}{2}\mu\int \overline{(H_x-iH_y)^2\omega'(\sigma)d\sigma}
\end{aligned}
\tag{B1}
$$

where $\bar\sigma = 1/\sigma$ and (13) are used. It is also used that H_θ is a real function and $H_r = 0$ on the boundary surface S_3. This form (B1) of the boundary condition was given in Hasebe et al. (2001, 2007).

Using this boundary condition, another stress function is obtained as follows:

$$
\Psi_a(\zeta) = -\overline{\Phi_a}\left(\frac{1}{\zeta}\right) - \frac{\bar\omega(1/\zeta)}{\omega'(\zeta)}\Phi_a'(\zeta) - \frac{1}{2}\mu\int (H_x-H_y)^2\omega'(\zeta)d\zeta \tag{B2}
$$

Substituting (B2) into (29), it is noticed that the magnetic stresses are calculated by the following equations:

$$
\begin{aligned}
&\sigma_x+\sigma_y = 4Re\left[\Phi_a'(\zeta)/\omega'(\zeta)\right] \\
&\sigma_y-\sigma_x+2i\tau_{xy} = 2\left[\overline{\omega(\zeta)}\left(\frac{\Phi_a'(\zeta)}{\omega'(\zeta)}\right)'\frac{1}{\omega'(\zeta)}+\frac{\Psi\prime_a(\zeta)}{\omega'(\zeta)}\right] \\
&\Phi_a(\zeta) = -1/2\mu^{(2)}H_0^2\sin^2\alpha_1 F_0 e^{2i\gamma}/\zeta \equiv \tau_0 F_0 e^{2i\gamma}/\zeta \\
&\Psi_a(\zeta) = -\overline{\Phi_a}\left(\frac{1}{\zeta}\right) - \frac{\bar\omega(1/\zeta)}{\omega'(\zeta)}\Phi_a'(\zeta)
\end{aligned}
\tag{B3a, b, c, d}
$$

The terms regarding Maxwell stress (terms of $\mu(H_x - iH_y)^2$ in (29b), (42) and (B2)) are not included, and it is noticed that the magnetic stress components of stress state (a) are the same as the stress functions subjected to the pure shear stress $-\mu H_0^2\sin^2\alpha_1/2 \equiv \tau_0$ (Hasebe and Ueda, 1980), or of the superposition of stress states subjected to compressive and tensile stresses in the γ direction of the magnetic field and in the perpendicular to the γ direction, respectively. The same thing above was mentioned in Hasebe (2010a). Therefore stress state (a) for the thin plate with an arbitrary shaped hole under uniform magnetic field is given by the result of Hasebe et al. (2001, 2007).

References

Hasebe, N., 2010a. Magnetic field and magneto elastic stress in an infinite plate containing an elliptical hole with an edge crack under uniform electric current. Int. J. Solid Struct. 47, 3374–3411.

Hasebe, N., 2010b. Magneto-elastic stress in a thin infinite plate with an elliptical hole under uniform magnetic field. Arch. Appl. Mech.

Hasebe, N., Horiuchi, Y., 1978. Stress analysis for a strip with semi-elliptical notches of crack on both sides by means of rational mapping function. Ing. Arch. 47 (3), 169–179.

Hasebe, N., Inohara, S., 1981. Stress intensity factor at a bilaterally-bent crack in the bending problem of thin plate. Eng. Fract. Mech. 14 (3), 607–616.

Hasebe, N., Ueda, M., 1980. Crack originating from a corner of a square hole. Eng. Fract. Mech. 13 (4), 913–928.

Hasebe, N., Wang, X.F., 2005. Complex variable method for thermal stress problem. J. Therm. Stresses 28, 595–648.

Hasebe, N., Matsuura, S., Kondo, N., 1984. Stress analysis of a strip with a step and a crack. Eng. Fract. Mech. 20 (3), 447–462.

Hasebe, N., Sugimoto, T., Nakamura, T., 1986a. Longitudinal shear problem for an elastic body with two fixed edges. J Appl. Mech. (ASME) 53 (4), 814–818.

Hasebe, N., Tamai, K., Nakamura, T., 1986b. Analysis of a kinked crack under uniform heat flow. J. Eng. Mech. (ASCE) 112 (1), 31–42.

Hasebe, N., Wang, X.F., Nakanishi, H., 2001. Analysis of magnet-elastic problem for infinite plate containing cracked hole. Developments in Fracture Mechanics for the New Century. Society of Materials Science, Japan.

Hasebe, N., Wang, X.F., Nakanishi, H., 2007. On magneto-elastic problems of a plane with an arbitrarily shaped hole under stress and displacement boundary conditions. Q. J. Mech. Appl. Math. 60, 423–442.

Hasebe, N., Jin, X., Keer, L.M., Wang, Q., 2008. Electromagnetic fields induced by electric current in an infinite plate with an elliptical hole. Q. J. Mech. Appl. Math. 61, 615–633.

Moon, F.C., 1984. Magneto-solid Mechanics. John Wiley, New York.

Muskhelishvili, N.I., 1963. Some Basic Problems of the Mathematical Theory of Elasticity. Noordhoff, Groningen.

Paria, G., 1967. Magneto-elasticity and magneto-thermo-elasticity. In: Chernyi, G.C. (Ed.), Advances in Applied Mechanics, vol. 10. Academic Press, New York, pp. 73–112.